IEEE Access
Multidisciplinary ⋮ Rapid Review ⋮ Open Access Journal

Received 21 February 2023, accepted 18 April 2023, date of publication 11 May 2023, date of current version 24 May 2023.

Digital Object Identifier 10.1109/ACCESS.2023.3275170

RESEARCH ARTICLE

Phase Matching in Microstructured Lithium Niobate on Insulator Waveguides

NOR ROSHIDAH YUSOF[1,2], NORSHAMSURI ALI[1,2], (Senior Member, IEEE), PIOTR KOLENDERSKI[3], KAROLINA SŁOWIK[3], ROSDISHAM BIN ENDUT[1,2], AND SYED ALWEE ALJUNID SYED JUNID[1,2]

[1]Faculty of Electronic Engineering Technology, Universiti Malaysia Perlis, Arau, Perlis 02000, Malaysia
[2]Advanced Communication Engineering Centre of Excellent, UniMAP, Arau, Perlis 02000, Malaysia
[3]Faculty of Physics, Astronomy and Informatics, Institute of Physics, Nicolaus Copernicus University, 87-100 Toruń, Poland

Corresponding authors: Nor Roshidah Yusof (roshidahyusof@unimap.edu.my) and Piotr Kolenderski (kolenderski@umk.pl)

This work was supported in part by the Long Term Research Grant Scheme through the Fault-Tolerant Photonic Quantum States for Quantum Key Distribution Provided by the Ministry of Higher Education of Malaysia (MOHE) under Grant LRGS/1/2020/UM/01/5/2 and Grant 9012-00009; in part by the Horizon Europe; in part by the European Union's Framework Programme for Research and Innovation SEQUOIA Project 101070062; and in part by the National Centre for Research and Development, Poland, within the QUANTERA II Programme under Project QUANTERAII/1/21/E2TPA/2023.

ABSTRACT The recent development of the Lithium Niobate on Insulator (LNOI) fabrication process has opened a bright future for integrating ultra-compact photonic circuits. Due to its excellent nonlinear properties, as a waveguide material, Lithium Niobate supports nonlinear optical processes including efficient sum frequency generation and second harmonic generation. To enhance these effects, precise control of mode confinement and modal phase matching is required. In this work, we engineer an LNOI waveguide to match the effective refractive indices of the fundamental mode, TE_{00} at the fundamental wavelength and second-order mode, TE_{20} at the second harmonic wavelength. As waveguide geometry plays an essential role, optimization of waveguide parameters is crucial for the design of high-performance, feasible devices. Here, we numerically engineer and characterize the influence of rib waveguide geometry parameters including etching depth, D, width, W and sidewall angle, θ on the phase matching condition. We find that the waveguide phase matching condition is most susceptible to variations in the sidewall angle. For the optimized parameter values of $\{D, \theta\} = \{450\,\text{nm}, 10^o\}$, the phase-matching wavelength tunability is achieved through the waveguide width control.

INDEX TERMS Lithium niobate, LNOI, waveguide, phase matching, second harmonic generation.

I. INTRODUCTION

PHOTONIC integrated circuits (PIC) hold promise as a technology capable of overcoming the limitations of conventional electronic-based integrated circuits. By integrating multiple photonic components - such as light sources, modulators, detectors, and optical waveguides - onto a single chip, PICs harness photonics principles to manipulate and control light for a range of applications. Lithium Niobate (LN) is a prominent material platform for implementing PICs, as it boasts several favourable properties, including a strong electro-optic response, large refractive index, and wide transparency window spanning 400 to 5000 nm [1]. These properties make LN ideal for fabricating optical devices in PICs such as electro-optic modulators [2], optical waveguides [3], [4], nanocavities [5], and sensors [6]. While most devices have been fabricated using established Titanium diffusion [7], and proton exchange [8] methods, these conventional techniques cannot be used for ultra-compact and high-density device integration due to weak field confinement caused by low refractive index contrast [9]. Realizing nanophotonic devices has remained challenging until the recent development and commercialization of Lithium Niobate on Insulator (LNOI) techniques [10], which are similar to Silicon on Insulator

The associate editor coordinating the review of this manuscript and approving it for publication was David Caplan.

except for the thin film LN layer deposited on top of the silica-LN substrate. The thickness of this LN layer ranges from 300 to 800 nm [11].

Compared to bulk LN devices, LNOI offers huge benefits including footprint reduction, significant field enhancement as well as minimum propagation losses. The associated high refractive index contrast and a high degree of flexibility during the fabrication process enable the implementation of large-scale PICs for quantum photonic applications [12], [13]. These applications include the efficient generation of entangled photon pairs [14], efficient frequency conversion [15] and modulation, as well as precise photon detection. These effects can be realized by exploiting the exceptional properties of LNOI [16], [17] which rely on the phase matching condition. The condition can be relaxed through the quasi-phase matching in periodically poled structures, which allows the compensation of the phase mismatch due to the refractive index dispersion by periodically arranged domains of the LNOI crystal [18], [19]. Unfortunately, this domain inversion process requires high voltage and remains challenging. Alternatively, geometrical optimization through numerical engineering prior to fabrication may enable precise phase matching without periodic polling. Selected previous works adopt the inverse design approach by adjusting a small set of parameters to achieve desired optical and functional characteristics of a device [20], [21]. In this paper, we perform comprehensive numerical work which involves geometrical waveguide optimization in order to obtain perfect phase-matching.

We focus on a z-cut LNOI rib waveguide of a trapezoidal cross-section. Similar geometries have been discussed before in the context of lateral leakage engineering [3]. Experimentally feasible [22], [23], [24], they have been discussed [25] and exploited for efficient second harmonic generation [4], [19]. Here, we investigate the waveguide in the context of phase matching. We identify the pair of modes at the fundamental and second harmonic wavelength that fulfils the phase-matching condition. The influence of the height, width and sidewall angle of the core on modal properties is studied. We optimize waveguide parameters to achieve the perfect phase-matching condition. We determine the geometrical factors to variations of which the phase matching condition is most susceptible. Consequently, we discuss the phase matching wavelength tunability through variation of the core width to cover the S to L band telecommunication wavelength region ranging from 1450 to 1625 nm. The waveguide engineered in this manuscript may potentially be integrated as an element of a PIC.

II. DESIGN AND SIMULATION

Our waveguide design is performed using the commercial Comsol Multiphysics software based on the finite element method [26]. We assume an infinitely long waveguide allowing us to exploit the 2D geometry setting. As depicted in the cross-sectional view in Fig. 1, the waveguide consists of a core and a thin LN slab underneath, which enables strong modal confinement. The width of the core is W, and the height $H = D + h$, where D stands for the etching depth and h for the slab height. The core thickness is 500 nm. The structure is deposited on a SiO_2 - LN substrate and cladded with a 2 μm thick conformal layer of SiO_2 to minimize the influence of surface contamination and to provide isolation [27]. The ordinary and extraordinary refractive indices of the congruent LN are evaluated based on the Sellmeier equations [28], [29], which describe the dispersion relation in the material, and the refractive index of SiO_2 (n_{SiO2}=1.44). The maximum triangular meshing size is set to be one-fifth of the operating wavelength for the optimal computational processing time [26]. The inset in the bottom-right of Fig. 1 shows the orientation of the principal dielectric axes with respect to the optical waveguide. In this case, the z-cut LNOI allows transverse field propagation along the y-axis and confinement in xz-plane. This geometrical design supports both transverse electric (TE) and magnetic (TM) modes. Nevertheless, the TE mode profile which is polarized along the x-axis is further investigated to access the largest nonlinear coefficient (d_{33}) [30].

A. MODAL PHASE MATCHING

Our first goal is to achieve the phase matching condition for the fundamental mode, TE_{00} at 1550 nm and the second-order mode, TE_{20} at second harmonic wavelength of 775 nm. The modal propagation through the waveguide is characterized by the effective refractive indices, $n_{\text{eff}} = \frac{\beta_0}{k_0}$, where β_0 and k_0 denote the propagation constant and free space wavenumber, respectively. Fig. 2 shows the dependence of the effective indices on the waveguide width, W for the fundamental mode, $TE_{00,1550}$ and the first three higher-order modes ($TE_{00,775}$, $TE_{10,775}$, $TE_{20,775}$). Generally, the value of n_{eff} is increased for broader width. Compared to $TE_{00,1550}$, $TE_{00,775}$ is characterized with a value of n_{eff} higher by 0.3856 at $W = 500$ nm. The difference is reduced significantly to 0.2118 as the width of core is increased from 500 to 1500 nm. In this case, $TE_{00,775}$ supports a stronger modal confinement as the n_{eff} value is closer to n_{LN}. Nevertheless, the higher order modes at the second harmonic wavelength, $TE_{10,775}$ and $TE_{20,775}$ posses lower n_{eff} values. The first effective index overlap is found for the $TE_{00,1550}$ and $TE_{20,775}$ modes at $\{W, n_{\text{eff}}\} = \{975\,\text{nm}, 1.889\}$, where the perfect modal phase matching condition is achieved. Contrarily, overlapping of indices for the $TE_{00,1550}$ and $TE_{00,775}$ modes is hardly achieved due to the existence of material and waveguide dispersion. Hence, the following discussion shall consider the interaction of $TE_{00,1550}$ and $TE_{20,775}$ modes.

As reported in previous works, the number of supported modes and modal confinement in a rib waveguide is highly dependent on its geometrical structure [31], [32]. This is represented by the following relations:

$$\frac{W}{H} \geq 0.3 + \frac{r}{\sqrt{1 - r^2}} \quad \text{for } 0.5 \geq r \geq 1.0 \tag{1}$$

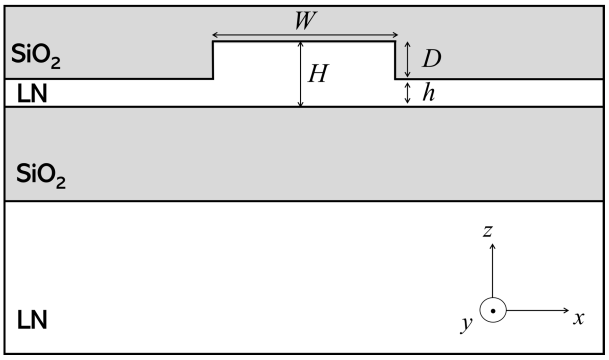

FIGURE 1. Cross-sectional view of the *z*-cut LNOI rib waveguide investigated in this work.

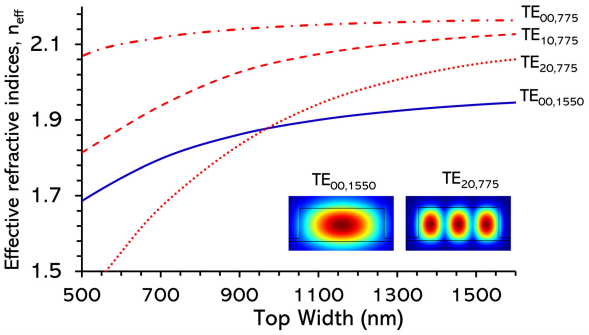

FIGURE 2. Effective refractive indices, n_{eff} for the first four modes as functions of the width of core, *W* ranging from 500 to 1500 nm. The blue solid line and the red lines (solid, dotted, dashed) indicate the effective mode indices of the fundamental and second harmonic wavelengths, respectively. The inset figures show the fundamental and second-order transverse electric field mode profiles at the corresponding wavelengths.

$$\frac{W}{H} \geq 0.05 + \frac{(0.94 + 0.25H)r}{\sqrt{1 - r^2}} \quad \text{for } 0 \geq r \geq 0.5 \qquad (2)$$

where $r = h/H$. The first equation is the single mode condition in Silicon on insulator rib waveguide of large dimension, while the latter relation corresponds to relatively small rib structures. We extend our analysis to investigate the influence of this geometrical parameter on the phase-matching condition.

For this purpose, we vary the etching depth, $D = H(1 - r)$ from 320 nm to 480 nm, which corresponds to the decrement of slab thickness, h from 180 to 20 nm. It also represents the transition of shallowly etched towards deeply etched rib waveguide structure. In parallel, the ratio r is reduced from 0.3 to 0.04. As depicted in Fig.3, the index overlap between $\text{TE}_{00,1550}$ and $\text{TE}_{20,775}$ is observed for $D > 350$ nm. In shallowly etched waveguides, the phase matching condition in hard to be achieved mainly due to the mode leakage on the slab. At $D = 350$ nm corresponding to $h/H = 0.3$, the phase matching condition is achieved at $W_{\text{PM}} = 830$ nm. The value of W_{PM} linearly increases with an average slope of 2.6 for the etching depths in the range of $D \in (350, 400)$ nm. Increasing the etching depth to values higher than 400 nm eventually leads to an insignificant variation of W_{PM}. On top

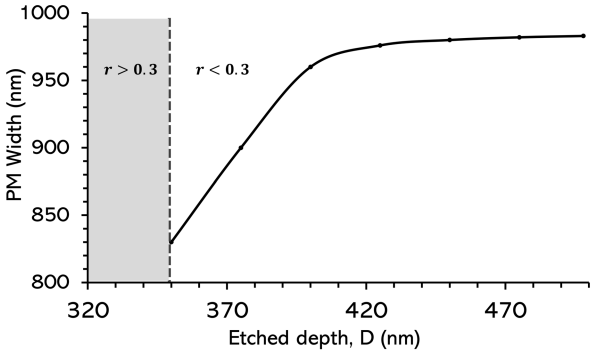

FIGURE 3. Influence of etching depth on phase-matching top width as we set a fixed value of $H = 500$ nm.

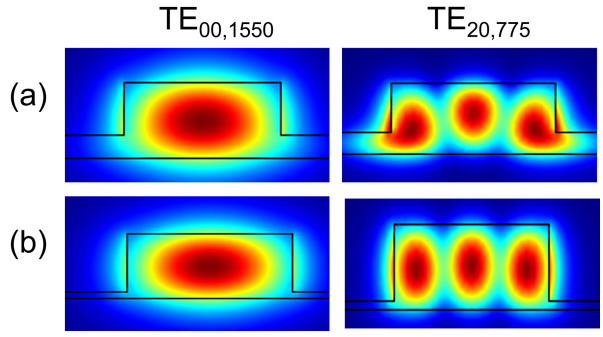

FIGURE 4. $\text{TE}_{00,1550}$ and $\text{TE}_{20,775}$ mode profile variation for etching depth *D* of (a) 350 nm and (b) 450 nm.

of that, it can be seen that the deeply etched rib structures with $D \in (350, 450)$ nm sustain tight mode confinement and compact effective mode areas, as shown in Fig. 4. The small effective area enhances coupling and conversion efficiency between the fundamental and second harmonic wavelengths.

The major constraint for nanostructuring LNOI waveguides lies in the chemically inert properties of Lithium Niobate which make the fabrication of vertical rib waveguides challenging [22]. The complicated technique of dry etching allows the fabrication of trapezoidal waveguides which shifts the phase matching width W_{PM}. Hence, it is interesting to investigate the effect of sidewall angle variation on the phase-matching condition. We thus introduce the sidewall angle as shown in the inset of Fig. 5. The bottom width $W_b = W_t + 2D \tan\theta$ of the core is then slightly broader than the top width W_t. At $\theta = 0^o$, results for the vertical waveguide replicate the ones presented in Fig.3 with $W_b = W_t = W_{\text{PM}}$. For trapezoidal waveguides, the W_{PM} is found to decrease linearly with the sidewall angle (Fig. 5). Intriguingly, increasing the etched depth to $D = 450$ nm allows a variation of angle up to 25^o, which is out of reach for the same range of waveguide widths at lower etching depth of $D = 350$ and 400 nm. Increasing the angle higher than this value may lead to mode hybridization, where two orthogonally polarized modes sustain almost equal effective indices yet are anti-crossed with each other. This phenomenon occurs due to the perturbation caused by waveguide asymmetry, and is useful for the design of tapered

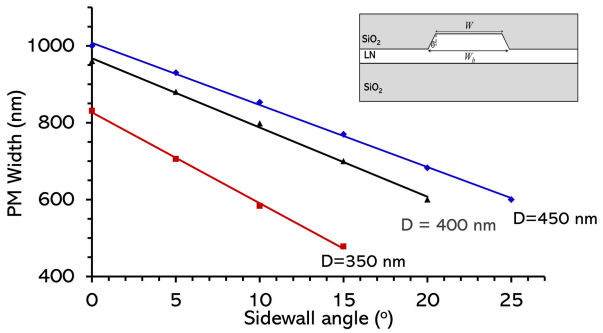

FIGURE 5. Linear relation of the phase matching width with sidewall angle for the etching depth of 350 nm (red), 400 nm (black) and 450 nm (blue).

waveguides for applications such as mode conversion and optical signal processing [33].

B. GEOMETRY OPTIMIZATION

To find the geometry which supports the second harmonic generation process, we performed numerical optimization of the phase mismatch, $\Delta n = n_{\mathrm{TE00,1550nm}} - n_{\mathrm{TE20,775\ nm}}$, with respect to the waveguide parameters, D, W and θ. The numerical evaluation of the values of effective refractive indices for a given waveguide parameters is very time consuming. Therefore, we are limited to 64 geometries yielding phase mismatch values very close to zero, see Table 1. These points are next used to build an interpolation function, $(\Delta n)^2$, which is in turn minimized over the geometry parameters. As a result, we obtained the optimal $D = 450$ nm, $W = 800$ nm and $\theta = 10°$.

Please note that numerical optimization of interpolating function based on the points simulated in COMSOL is a procedure that gives approximate results. In order to increase the precision one can perform new numerical simulation for the parameters found in the optimization process and update the interpolation function. This step can be repeated as long as the required precision is achieved.

C. PHASE MATCHING WAVELENGTH TUNABILITY

Fulfilment of the phase matching condition allows for efficient second harmonic generation and creation of entangled photon pairs in spontaneous parametric down conversion. The phase-matching wavelength at which the processes efficiently occur can be tuned through engineering of the waveguide width, as we demonstrate below.

We fix the etching depth and the sidewall angle at the optimal values of $\{D, \theta\} = \{450\,\mathrm{nm}, 10^o\}$. We investigate the phase matching between the effective indices $n_{\mathrm{TE00,FF}}$ and $n_{\mathrm{TE20,SH}}$, where the FF and SH subscripts indicate the fundamental and the second harmonic modes, with the wavelengths $\lambda_{\mathrm{SH}} = \frac{\lambda_{\mathrm{FF}}}{2}$. In our analysis λ_{FF} ranges from 1350 to 1750 nm. The refractive index difference is shown in Fig. 6, in which the blue areas correspond to the Δn values up to 0.01. The found relation between the phase matching wavelength and

TABLE 1. Simulated geometries and their respective phase mismatch.

1	350	700	0	0.0220
2	350	700	5	0.0525
3	350	700	10	0.0207
4	350	700	15	0.0116
5	350	800	0	0.0280
6	350	800	5	0.0433
7	350	800	10	0.0300
8	350	800	15	0.0350
9	350	900	0	0.0392
10	350	900	5	0.0340
11	350	900	10	0.0392
12	350	900	15	0.0431
13	350	1000	0	0.0374
14	350	1000	5	0.0450
15	350	1000	10	0.0400
16	350	1000	15	0.0350
17	370	700	0	0.0538
18	370	700	5	0.0480
19	370	700	10	0.0426
20	370	700	15	0.0388
21	370	800	0	0.0250
22	370	800	5	0.0324
23	370	800	10	0.0305
24	370	800	15	0.0318
25	370	900	0	0.0239
26	370	900	5	0.0256
27	370	900	10	0.0315
28	370	900	15	0.0397
29	370	1000	0	0.0289
30	370	1000	5	0.0386
31	370	1000	10	0.0661
32	370	1000	15	0.0567
33	400	700	0	0.0710
34	400	700	5	0.0705
35	400	700	10	0.0371
36	400	700	15	0.0186
37	400	800	0	0.0563
38	400	800	5	0.0407
39	400	800	10	0.0272
40	400	800	15	0.0001
41	400	900	0	0.0018
42	400	900	5	0.0196
43	400	900	10	0.0155
44	400	900	15	0.0236
45	400	1000	0	0.0202
46	400	1000	5	0.0500
47	400	1000	10	0.0433
48	400	1000	15	0.0534
49	450	700	0	0.0571
50	450	700	5	0.1337
51	450	700	10	0.0184
52	450	700	15	0.0017
53	450	800	0	0.03500
54	450	800	5	0.1170
55	450	800	10	0.0010
56	450	800	15	0.0247
57	450	900	0	0.0117
58	450	900	5	0.0102
59	450	900	10	0.0193
60	450	900	15	0.0293
61	450	1000	0	0.0416
62	450	1000	5	0.02700
63	450	1000	10	0.0398
64	450	1000	15	0.0511

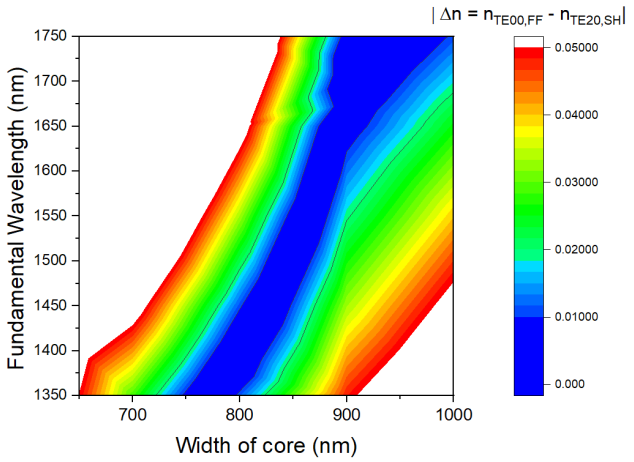

FIGURE 6. Refractive index difference between the fundamental and second-harmonic modes over the width of core and fundamental wavelength at $\{D, \theta\} = \{450\,\text{nm}, 10^{o}\}$.

waveguide width is to a good approximation linear. The range of waveguide widths between 750 and 950 nm supports phase matching in the range of 1350 to 1750 nm. Nevertheless, a minimum waveguide width of 850 nm is required to support the S up to L telecommunication band. It is also depicted that the $\Delta\lambda$ increases towards broader waveguide widths, with the maximum $\Delta\lambda$ found at $W = 900$ nm. On top of that, the wider width tolerance, ΔW are accessible for longer wavelength with the maximum ΔW reported at $\lambda_{FF} = 1750$ nm.

III. CONCLUSION

In this work, a wide range of widths, etching depths and sidewall angles of an LNOI rib waveguide has been systematically investigated and optimized to fulfil the phase-matching condition. The difference between effective refractive indices of the $TE_{00,1550}$ and $TE_{20,775}$ modes has been thoroughly analysed over these geometrical parameters' variations. We found that phase matching can only be achieved in rib waveguides with large etching depths. This finding is in agreement with the large cross-sectional SOI rib waveguide equation proposed by Soref [31]. Nonzero sidewall angles of the rib waveguide result in asymmetrical mode profiles as well as a shift of the phase-matching width into smaller values. Optimal phase matching has been predicted at $\{D, W, \theta\} = \{450\,\text{nm}, 800\,\text{nm}, 10^{o}\}$. The analysis has been extended to investigate the phase-matching wavelength tunability with the waveguide width. Interestingly, with the widths ranging from 750 to 950 nm the phase matching can be achieved within the telecommunication range.

Our findings have implications for various fields: The advancement of phase matching studies in LNOI rib waveguides contributes to the progress of nonlinear optical signal processing. By achieving phase matching between interacting optical modes, a range of nonlinear signal processing functionalities can be achieved, including all-optical switching, wavelength conversion, and pulse shaping. These functionalities play a vital role in high-speed optical communication systems and advanced modulation formats. Furthermore, the ability to achieve phase matching between different optical modes enables the manipulation of quantum states of light, leading to the realization of efficient and robust quantum photonic devices such as quantum gates, quantum memories, and single-photon sources. Finally, the frequency conversion allows for the generation of coherent light at new wavelengths to be used in spectroscopy and imaging technology.

CONFLICT OF INTEREST STATEMENT

The authors declare that the research was conducted without any commercial or financial relationships that could be construed as a potential conflict of interest.

AUTHOR CONTRIBUTIONS

Conceptualization, Nor Roshidah Yusof and Norshamsuri Ali; validation, Piotr Kolendersk, Karolina Słowik, and Nor Roshidah Yusof; writing-original draft preparation, Nor Roshidah Yusof and Norshamsuri Ali; writing-review and editing, all authors. All authors have read and agreed to the published version of the manuscript.

ACKNOWLEDGMENT

The authors would like to thank Dr. Ahmad Rifqi for the support and knowledge sharing related to this project.

REFERENCES

[1] L. Arizmendi, "Photonic applications of lithium niobate crystals," *Phys. Status Solidi A*, vol. 201, no. 2, pp. 253–283, Jan. 2004.
[2] P. Ying, H. Tan, J. Zhang, M. He, M. Xu, X. Liu, R. Ge, Y. Zhu, C. Liu, and X. Cai, "Low-loss edge-coupling thin-film lithium niobate modulator with an efficient phase shifter," *Opt. Lett.*, vol. 46, no. 6, pp. 1478–1481, 2021.
[3] A. Boes, L. Chang, M. Knoerzer, T. G. Nguyen, J. D. Peters, J. E. Bowers, and A. Mitchell, "Improved second harmonic performance in periodically poled LNOI waveguides through engineering of lateral leakage," *Opt. Exp.*, vol. 27, no. 17, pp. 23919–23928, 2019.
[4] R. Luo, Y. He, H. Liang, M. Li, and Q. Lin, "Highly tunable efficient second-harmonic generation in a lithium niobate nanophotonic waveguide," *Optica*, vol. 5, no. 8, pp. 1006–1011, Aug. 2018.
[5] H. Liang, R. Luo, Y. He, H. Jiang, and Q. Lin, "High-quality lithium niobate photonic crystal nanocavities," *Optica*, vol. 4, no. 10, pp. 1251–1258, 2017.
[6] W. Sohler, "Integrated optical devices in lithium niobate," *Opt. Photon. News*, vol. 19, no. 1, pp. 24–31, 2008.
[7] R. Schmidt and I. Kaminow, "Metal-diffused optical waveguides in $LINBO_3$," *Appl. Phys. Lett.*, vol. 25, no. 8, pp. 458–460, 1974.
[8] G. R. Paz-Pujalt, D. D. Tuschel, G. Braunstein, T. Blanton, S. T. Lee, and L. M. Salter, "Characterization of proton exchange lithium niobate waveguides," *J. Appl. Phys.*, vol. 76, no. 7, pp. 3981–3987, Oct. 1994.
[9] Y. Qi and Y. Li, "Integrated lithium niobate photonics," *Nanophotonics*, vol. 9, no. 6, pp. 1287–1320, Jun. 2020.
[10] G. Poberaj, H. Hu, W. Sohler, and P. Günter, "Lithium niobate on insulator (LNOI) for micro-photonic devices," *Laser Photon. Rev.*, vol. 6, no. 4, pp. 488–503, Jul. 2012.
[11] A. Boes, B. Corcoran, L. Chang, J. Bowers, and A. Mitchell, "Status and potential of lithium niobate on insulator (LNOI) for photonic integrated circuits," *Laser Photon. Rev.*, vol. 12, no. 4, Apr. 2018, Art. no. 1700256.
[12] S. Saravi, T. Pertsch, and F. Setzpfandt, "Lithium niobate on insulator: An emerging platform for integrated quantum photonics," *Adv. Opt. Mater.*, vol. 9, no. 22, Nov. 2021, Art. no. 2100789.

[13] E. Pelucchi, G. Fagas, I. Aharonovich, D. Englund, E. Figueroa, Q. Gong, H. Hannes, J. Liu, C.-Y. Lu, N. Matsuda, J.-W. Pan, F. Schreck, F. Sciarrino, C. Silberhorn, J. Wang, and K. D. Jöns, "The potential and global outlook of integrated photonics for quantum technologies," *Nature Rev. Phys.*, vol. 4, no. 3, pp. 194–208, Dec. 2021.

[14] G.-T. Xue, Y.-F. Niu, X. Liu, J.-C. Duan, W. Chen, Y. Pan, K. Jia, X. Wang, H.-Y. Liu, Y. Zhang, P. Xu, G. Zhao, X. Cai, Y.-X. Gong, X. Hu, Z. Xie, and S. Zhu, "Ultrabright multiplexed energy-time-entangled photon generation from lithium niobate on insulator chip," *Phys. Rev. Appl.*, vol. 15, no. 6, Jun. 2021, Art. no. 064059.

[15] A. Boes, L. Chang, T. Nguyen, G. Ren, J. Bowers, and A. Mitchell, "Efficient second harmonic generation in lithium niobate on insulator waveguides and its pitfalls," *J. Phys., Photon.*, vol. 3, no. 1, Jan. 2021, Art. no. 012008.

[16] E. Lomonte, M. A. Wolff, F. Beutel, S. Ferrari, C. Schuck, W. H. P. Pernice, and F. Lenzini, "Single-photon detection and cryogenic reconfigurability in lithium niobate nanophotonic circuits," *Nature Commun.*, vol. 12, no. 1, pp. 1–10, Nov. 2021.

[17] Y.-X. Lin, C.-H. Lee, H.-P. Chung, M. Younesi, P. Kumar, K. Wang, O. Bernard, C. Shirpurkar, W.-C. Su, R. Geiss, T. Pertsch, A. Sukhorukov, F. Setzpfandt, and Y.-H. Chen, "Integrated photonic sources and circuits in lithium niobate platform," in *Proc. Optoelectronics Commun. Conf.*, 2021, p. 2.

[18] J.-Y. Chen, C. Tang, Z.-H. Ma, Z. Li, Y. M. Sua, and Y.-P. Huang, "Efficient and highly tunable second-harmonic generation in Z-cut periodically poled lithium niobate nanowaveguides," *Opt. Lett.*, vol. 45, no. 13, pp. 3789–3792, 2020.

[19] H. Zhang, Q. Li, H. Zhu, L. Cai, and H. Hu, "Second harmonic generation by quasi-phase matching in a lithium niobate thin film," *Opt. Mater. Exp.*, vol. 12, no. 6, pp. 2252–2259, 2022.

[20] P. R. Wiecha, A. Arbouet, C. Girard, and O. L. Muskens, "Deep learning in nano-photonics: Inverse design and beyond," *Photon. Res.*, vol. 9, no. 5, p. B182, 2021.

[21] K. Yao, R. Unni, and Y. Zheng, "Intelligent nanophotonics: Merging photonics and artificial intelligence at the nanoscale," *Nanophotonics*, vol. 8, no. 3, pp. 339–366, Mar. 2019.

[22] I. Krasnokutska, J.-L. J. Tambasco, and A. Peruzzo, "Nanostructuring of LNOI for efficient edge coupling," *Opt. Exp.*, vol. 27, no. 12, pp. 16578–16585, 2019.

[23] I. Krasnokutska, J.-L. J. Tambasco, X. Li, and A. Peruzzo, "Ultra-low loss photonic circuits in lithium niobate on insulator," *Opt. Exp.*, vol. 26, no. 2, pp. 897–904, 2018.

[24] R. Takigawa, E. Higurashi, T. Kawanishi, and T. Asano, "Lithium niobate ridged waveguides with smooth vertical sidewalls fabricated by an ultraprecision cutting method," *Opt. Exp.*, vol. 22, no. 22, pp. 27733–27738, 2014.

[25] L. Wang, L.-Q. Li, X.-T. Zhang, and F. Chen, "Type i phase matching in thin film of lithium niobate on insulator," *Results Phys.*, vol. 16, Mar. 2020, Art. no. 103011.

[26] H. C. Lim, *Optics Modeling and Visualization With COMSOL Multiphysics*. Stockholm, Sweden: COMSOL AB, 2018.

[27] M. M. Milosevic, P. S. Matavulj, B. D. Timotijevic, G. T. Reed, and G. Z. Mashanovich, "Design rules for single-mode and polarization-independent silicon-on-insulator rib waveguides using stress engineering," *J. Lightw. Technol.*, vol. 26, no. 13, pp. 1840–1846, Jul. 1, 2008.

[28] D. E. Zelmon, D. L. Small, and D. Jundt, "Infrared corrected sellmeier coefficients for congruently grown lithium niobate and 5 mol.% magnesium oxide–doped lithium niobate," *J. Opt. Soc. Amer. B, Opt. Phys.*, vol. 14, no. 12, pp. 3319–3322, 1997.

[29] C. Z. Tan, "Determination of refractive index of silica glass for infrared wavelengths by IR spectroscopy," *J. Non-Crystalline Solids*, vol. 223, nos. 1–2, pp. 158–163, Jan. 1998.

[30] I. Briggs, S. Hou, C. Cui, and L. Fan, "Simultaneous type-I and type-II phase matching for second-order nonlinearity in integrated lithium niobate waveguide," *Opt. Exp.*, vol. 29, no. 16, pp. 26183–26190, 2021.

[31] R. A. Soref, J. Schmidtchen, and K. Petermann, "Large single-mode rib waveguides in GeSi-Si and Si-on-SiO/sub 2," *IEEE J. Quantum Electron.*, vol. 27, no. 8, pp. 1971–1974, 1991.

[32] S. P. Chan, C. E. Png, S. T. Lim, G. T. Reed, and V. M. N. Passaro, "Single-mode and polarization-independent silicon-on-insulator waveguides with small cross section," *J. Lightw. Technol.*, vol. 23, no. 6, pp. 2103–2111, Jun. 2005.

[33] A. Kaushalram, G. Hegde, and S. Talabattula, "Mode hybridization analysis in thin film lithium niobate strip multimode waveguides," *Sci. Rep.*, vol. 10, no. 1, pp. 1–13, Oct. 2020.

NOR ROSHIDAH YUSOF received the B.Sc. and M.Sc. degrees in physics from the University of Science Malaysia, Malaysia, in 2007 and 2010, respectively. She is currently pursuing the Ph.D. degree in photonic engineering with Universiti Malaysia Perlis (UniMAP), Malaysia. She has been a Lecturer with UniMAP, since 2011. Her research interests include optical waveguides, photonics, and quantum communication. She granted the scholarship from the Ministry of Higher Education Malaysia to pursue her Ph.D. studies. Throughout the study, she has published conference and journal articles, received several awards, and participated in scientific exchange programs, including the Research Excellence Award UniMAP, the Torun Astrophysics/Physics Summer Program, and the NAWA Academic Exchange Program.

NORSHAMSURI ALI (Senior Member, IEEE) is currently an Associate Professor with University Malaysia Perlis. Before joining UniMAP, in 2015, he lead and conduct the quantum and electronic project in MIMOS Berhad. He holds three WIPO patents for his work with MIMOS Berhad, all of which are based on the quantum systems. He has been working on quantum random number generators, quantum key distribution, quantum networks, QKD system prototypes, network security, and embedded systems. He focuses his work with UniMAP on quantum systems, electronics design, optical spectroscopy, and optical communication. Since 2015, he has been receiving research grants totaling close to RM 4.8 million. He also has 59 articles and 25 of which are in journals. His group has received 16 gold medals and six special prizes in prestigious major research exhibitions both locally and globally. Currently, he supervises four M.Sc. students and six Ph.D. students, the majority of them are working on quantum projects and optical communication, both theoretical and experimental.

PIOTR KOLENDERSKI received the master's and Ph.D. degrees from Nicolaus Copernicus University (NCU), Toruń, Poland. He is currently an Associate Professor with the Institute of Physics, NCU. He pursued his postdoctoral fellowship with the Institute for Quantum Computing (IQC), Waterloo, Canada, as a Laureate of the "Mobility Plus" Program from the Ministry of Science and High Education of Poland. Since 2013, he has been an Associate Professor with the Institute of Physics, NCU, and leads the Single Photon Applications Laboratory, research group. His research interests include generation, detection and control the single photons and their applications for quantum communication, photon-matter interaction, and quantum optical coherence tomography. Apart from IQC, he cooperates with Politecnico di Milano, Italy, Palack University Olomouc, Czech Republic, Ulm University, Germany, and industry sector, Syderal Polska, Poland, Work Microwave GmbH, Germany, and Exatel, Poland.

KAROLINA SŁOWIK received the Ph.D. degree in atomic and optical physics in Toruń. She is currently an Associate Professor with the Institute of Physics, Nicolaus Copernicus University (NCU), Toruń, Poland. As a Postdoctoral Researcher, she is also with Friedrich Schiller University, Jena, and the Karlsruhe Institute of Technology, Germany, she expanded the scope of her scientific interests to include quantum nanophotonic and plasmonic systems. In 2016, she started the Quantum Nanooptics Theory Group, NCU, focusing on the interface of atomic physics, quantum optics, and nanophotonics. She received the Laureate of the 2019 Award of the Minister of Higher Education and Science, Poland, for Outstanding Young Scientists. She is a member of the AMOPD Board of the European Physical Society. She is also a PI of Polish and transnational research projects.

ROSDISHAM BIN ENDUT received the bachelor's degrees in telecommunication engineering from Universiti Malaya, Kuala Lumpur, in 2002, and the M.Sc. degree in communications and network engineering from Universiti Putra Malaysia, Selangor, in 2004. Currently, he is a Lecturer with the Department of Computer Engineering, Faculty of Electronic Engineering Technology, Universiti Malaysia Perlis. He is the author of one book, more than 37 articles, and more than ten inventions. His research interests include optical communication, optical spectroscopy, quantum communication, optical sensor, machine learning, and the Internet of Things applications. He is currently holding multiple intellectual property. His innovation has won research awards locally and internationally; ITEX, MTE, and SIIF in South Korea.

SYED ALWEE ALJUNID SYED JUNID is currently a Senior Professor with Universiti Malaysia Perlis (UniMAP). Throughout his career, he received numerous awards and published approximately 400 journals, proceedings, and books. He is appointed as a reviewer of several international journals in fibre optics and photonics. He had supervised and co-supervised 25 master's (M.Sc.) students and 33 Ph.D. students. His research interests include optical-orthogonal frequency division multiple (O-OFDM), wireless sensor networks, visible light communications (VLC), free space optic (FSO), hybrid or multi-dimensional OCDMA, OCDMA detection techniques, and fiber Bragg grating (FBG) optical sensors. He had secured a number of Science Fund Grants, FRGS, and PRGS from the Minister of High Education and International Grant from Salman bin Abdulaziz University, Saudi Arabia. He has an established Optical Communication Research Group that won many prestigious research awards locally and internationally; ITEX, SIIF, South Korea, INNOVA, Croatia, IENA Nuremberg, Germany, and British International Symposium (BIS), U.K.